Nanoscale Res Lett (2010) 5:1057–1062
DOI 10.1007/s11671-010-9602-5

NANO EXPRESS

Initial Growth of Single-Crystalline Nanowires: From 3D Nucleation to 2D Growth

X. H. Huang · G. H. Li · G. Z. Sun · X. C. Dou · L. Li · L. X. Zheng

Received: 9 February 2010 / Accepted: 2 April 2010 / Published online: 17 April 2010

Abstract The initial growth stage of the single-crystalline Sb and Co nanowires with preferential orientation was studied, which were synthesized in porous anodic alumina membranes by the pulsed electrodeposition technique. It was revealed that the initial growth of the nanowires is a three-dimensional nucleation process, and then gradually transforms to two-dimensional growth via progressive nucleation mechanism, which resulting in a structure transition from polycrystalline to single crystalline. The competition among the nuclei inside the nanoscaled-confined channel and the growth kinetics is responsible for the structure transition of the initial grown nanowires.

Keywords Nanowire · Electrodeposition · Anodic alumina membrane · Initial growth mechanism

X. H. Huang · G. H. Li (✉) · X. C. Dou · L. Li
Key Laboratory of Material Physics, Anhui Key Laboratory of Nanomaterials and Nanotechnology, Institute of Solid State Physics, Chinese Academy of Sciences, 230031 Hefei, People's Republic of China
e-mail: ghli@issp.ac.cn

G. Z. Sun · L. X. Zheng
School of Mechanical and Aerospace Engineering, Nanyang Technological University, Singapore, Singapore

Present Address:
X. H. Huang
Department of Electrical and Computer Engineering, National University of Singapore, Singapore, Singapore

Introduction

Single-crystalline nanowires are essential for the development of the functional nanodevices [1], and many approaches have been reported so far to synthesize nanowires, including chemical vapor deposition, hydrothermal synthesis, membrane-based fabrication, and so on [2–6]. Among these methods, the electrodeposition combined with anodic alumina membrane (AAM) is an effective method to fabricate various nanowires [7–11]. Many fancy concepts of nanodevices are based on nanowires with complex structure [12], and their realization is greatly relied on our knowledge about the detailed morphology control and growth mechanism of the nanowires.

The understanding of the initial nucleation and growth of nanomaterials is critical for their subsequent morphology and structure manipulation [13–15]. Alivisatos's group addressed this issue by using an in situ transmission electron microscope (TEM) technique, upon which some information on the in real growth and diffusion dynamics of nanocrystals was provided [16, 17]. Nevertheless, this technique cannot be used to study the growth of the electrodeposited nanowires. There are two cases in the growth of the nanowires using template-based electrodeposition strategy, the Au thin film served as electrode is either partly or fully covered the pores of the template. In the former case, Fukunaka's group found that Ni deposition initially yielded a hollow tube in each pore, and resulting in a structure transition from the tube to the wire at the growth front [18]. But in the later case, there is little report on the growth mechanism of the initial growth stage of the single-crystalline nanowires.

To shed some light on this later unresolved issue, the initial growth of the Sb and Co nanowires prepared by the pulsed electrodeposition into AAM was studied in this paper, and the growth mechanism was discussed.

Experimental

The AAM was prepared by a two-step anodization process as described in our previous report [11]. The Sb electrolyte is an aqueous solution consisted of 0.02 mol L^{-1} $SbCl_3$, 0.1 mol L^{-1} $C_6H_8O_7{\cdot}H_2O$, and 0.05 mol L^{-1} $K_3C_6H_5O_7{\cdot}H_2O$, and the Co electrolyte is an aqueous solution consisted of 0.05 mol L^{-1} $CoSO_4$ and 0.25 mol L^{-1} H_3BO_3, the pH value of both the electrolytes was adjusted to about two by adding appropriate amounts of 5 M H_2SO_4 solutions. Pulsed electrodeposition was performed in a common two-electrode plating cell at room temperature, and the deposition potential (U) is −1.0 V for Sb nanowires and −3.0 V for Co nanowires applied between graphite anode and AAM cathode. Both the pulse deposition time (T_{on}) and the delay time (T_{off}) between pulses are all 600 μs for Sb nanowires and 40 ms for Co nanowires. The current–time curve and Cyclic Voltammetry curve were measured by using an electrochemical workstation (CHI760C) with Ag/AgCl (saturated KCl) as reference electrode.

The samples were characterized by Philips X'Pert power X-ray diffractometer using Cu Kα($\lambda = 1.542$Å) radiation, field emission scanning electron microscopy (FESEM, FEI Sirion 200), and high-resolution transmission electron microscopy (HRTEM, JEM-2010) attached with selected area electron diffraction (SAED). For FE-SEM observation, the AAM was partially etched away by immersing the samples in an aqueous solution of 5% NaOH, and then washed with deionized water for several times. For TEM and HRTEM observations, the AAM was completely dissolved in a 5% NaOH solution, and then washed with distilled water several times, and finally dispersed in absolute ethanol by ultrasonic.

Results and Discussion

Figure 1 shows the XRD patterns of the top and bottom surfaces of the Sb nanowire array embedded in the AAM together with the standard diffraction peaks of Sb (JCPDF no.85-1324). One can see from the top surface diffraction (curve (1) in Fig. 1) that there is a very sharp diffraction peak at $2\theta = 41.98^{o}$, and other diffraction peaks are very weak, which indicates that almost all the nanowires have the same preferential growth orientation along the [110] direction of the rhombohedral Sb. The XRD pattern from the bottom surface (curve (2) in Fig. 1) of the nanowire array shows several other diffraction peaks besides the sharp (110) peak and two small peaks from Au, which shows that the initially formed Sb nanowires have different orientations. This result implies that the initial growth mode of Sb nanowires on the Au electrode might be a three-dimensional (3D) process. Meanwhile, the strong (110) diffraction in curve (2) indicates that the duration of the initial 3D growth is very short.

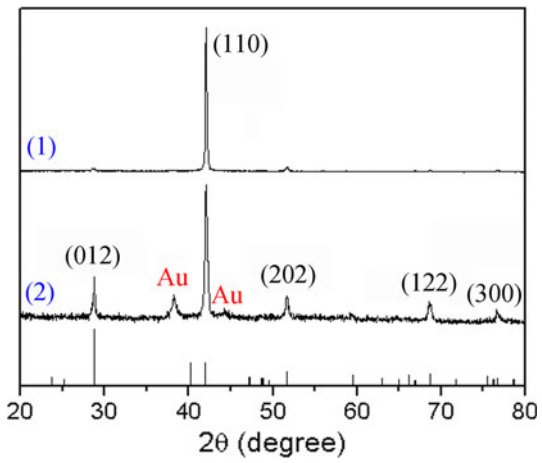

Fig. 1 XRD patterns of Sb nanowire array embedded in AAM: curve (1) *top surface and curve* (2) *bottom surface*. The diffraction peaks from Au electrode film marked with "Au" can be clearly seen in curve (2)

Figure 2 shows the FESEM images of the Sb nanowire array after partially etching away the AAM. Apparently, the top surface and side views (Fig. 2a–c) indicate that the high-filling Sb nanowires have almost the same height. As shown in the bottom side view (Fig. 2d), the bright particles residing on ends of the nanowires are originated from the Au electrode, which indicates that the contact between the nanowires and the Au films is compact, this is important for the reliability of the transport property as reported in previous work [11].

Figure 3 shows a typical TEM image of two parallel Sb nanowires removed from AAM, one can see the nanowires are uniform, smooth, and straight. The diameter of the Sb nanowires is about 40 nm, corresponding to the pore size of the AAM used. The different contrast along nanowires might originate from the deformation induced by the ultrasonic treatment used to prepare the TEM sample [19]. We can deduce that the darker part at the ends of the nanowires is Au from the physical basis of the image contrast in the TEM images (more clear in Fig. 4a), which has been further proved to be polycrystalline Au from the energy-dispersive spectrometer analysis attached to TEM and the SAED pattern (not show here). The appearance of Au electrode can be used as an indication of the initial growth part of Sb nanowires. The SAED patterns taken from the randomly selected regions marked by circles (1) and (2) along one single Sb nanowire clearly indicate that the nanowire is single crystalline in the areas a little far away from the Au electrode, while at the end of the nanowire on the Au electrode side shows a polycrystalline characteristic, which can be clearly seen from the SAED

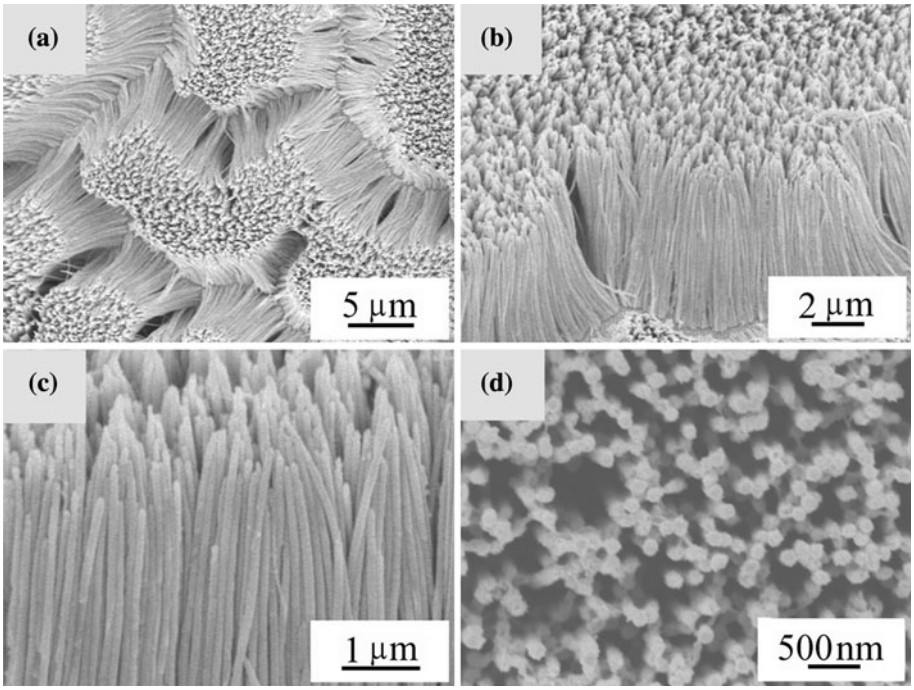

Fig. 2 FESEM images of Sb nanowire arrays: **a** *top surface view* **b–c** *side view* **d** *bottom surface view* of the Sb nanowire array

pattern from the end of the two nanowires on the Au electrode side marked by circle (3), indicating that the Sb nanowires formed in the initial growth stage are polycrystalline.

To further study the initial growth process, HRTEM observations were performed, as shown in Fig. 4. The HRTEM image taken from the ends of the nanowire closed to Au electrode, as shown in Fig. 4b, clearly shows that the lattice fringes derive from different crystalline grains. It is worthy to note that all the planes indexed here have also been observed in the XRD pattern in curve (2) of Fig. 1, which further proves the polycrystalline feature in the initial growth of the nanowire. The HRTEM images taken from areas along the nanowire growth direction till about 200 nm away from the end all show polycrystalline feature, as shown in Fig. 4c (the transition area). The HRTEM image taken from the area beyond 200 nm away from the end of the nanowire clearly shows 2D lattice fringes indicating the single-crystalline characteristic of the nanowire, as shown in Fig. 4d. This result indicates that the initial growth stage (or the transition length from polycrystalline to single crystalline) is about 200 nm. From Fig. 4d and its Fast Fourier Transform (FFT) image (see the inset), one also can see that the growth direction of Sb nanowire is along [110], which is consistent with the XRD and SAED results.

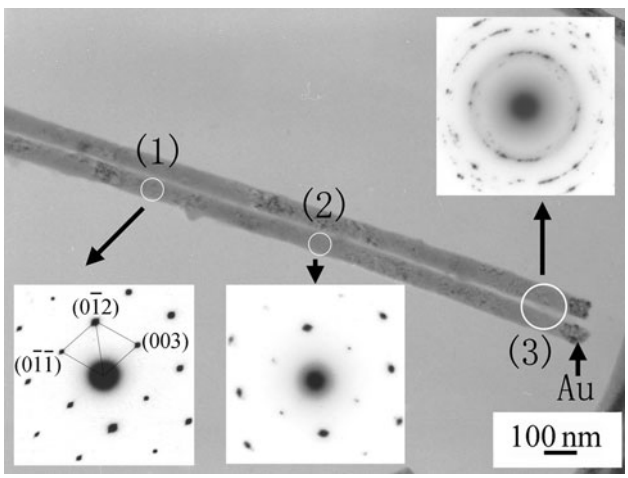

Fig. 3 TEM image of two parallel Sb nanowires and the corresponding SAED patterns in different areas. The areas (1) and (2) show the *single crystalline*, and the area (3) shows the *polycrystalline*

A similar phenomenon was observed in cubic Co nanowires. Figure 5a shows the XRD pattern of Co nanowire array. The inset of Fig. 5a is a FESEM image of the bottom side of the nanowires released from the pores of AAM, and rough surface on the tips of the nanowires can be seen. The intensity of the diffraction peak at $2\theta = 75.63^{o}$ is much stronger than the others, and it can be indexed to face-centered-cubic (FCC) Co [220] (JCPDS No. 89-4307) by combining TEM characterization. The other weak peaks can be indexed to FCC Co [111], Au [200] (JCPDS No. 89-3697), and HCP Co [10$\bar{1}$0] (labeled by "*", JCPDS No. 89-4308). Figure 5b shows a TEM image of a random selected individual Co nanowire. The SAED pattern taken from the tip of the nanowire shows some weak diffraction rings, and it was found that the diffraction rings correspond to polycrystalline Au electrode. The appearance of Au electrode also indicates the

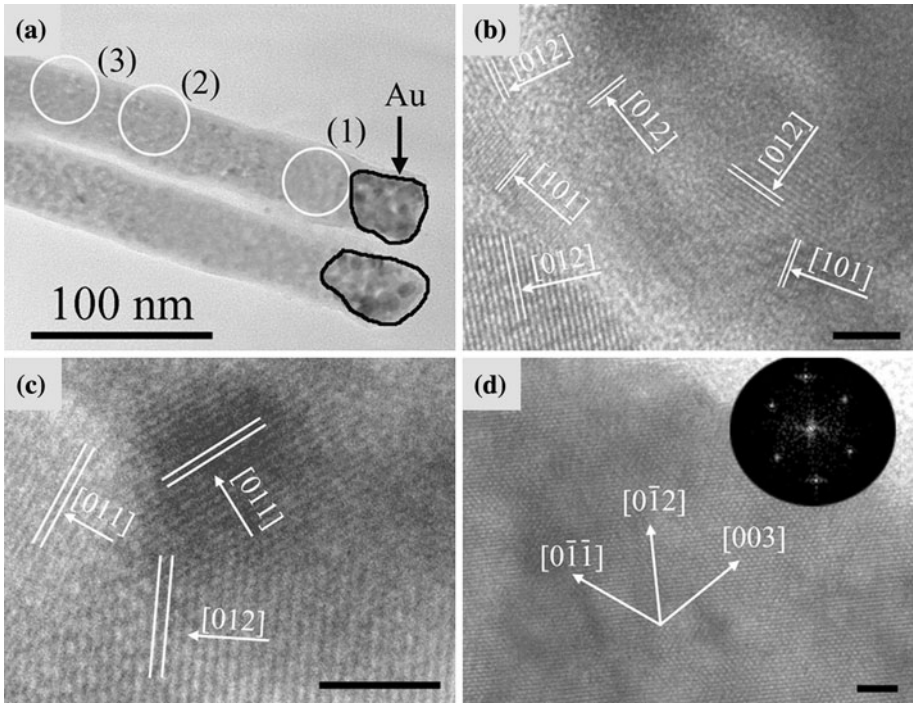

Fig. 4 **a** TEM image of *two parallel Sb nanowire* (the Au electrode film can be clearly seen at one end of the nanowire), **b**, **c** and **d** are HRTEM images of the areas marked (1), (2), and (3) in **a**, respectively. The inset in **d** is its FFT image. All the *scale bars* in **b**-**d** are 3 nm

initial growth of Co nanowires. As shown in the insets of Fig. 5b, the SAED pattern taken from the areas beyond 200 nm from Au electrode can be well indexed to single-crystalline FCC Co with orientation along [220] while that in the position near the Au electrode shows a polycrystalline characteristic. The mixture of the Au and Co signals in the SAED pattern is due to the fact that the electron-focused area is not small enough. These results also indicate that the Co nanowire formed in the initial growth stage is also polycrystalline and transforms into single crystalline in the subsequent growth.

In order to gain real-time information of the initial growth, the time evolution of the current during the electrodeposition of Co nanowires was measured. As shown in Fig. 6a, the deposition potential is switched between two states during the pulsed electrodeposition, the resulting transient pulsed current is shown in Fig. 6b. Metal ions are reduced at the deposition interface during T_{on}, resulting in a decrease of ion concentration, which is reflected by the decrease of current as shown in Fig. 6b during T_{on}. The current is negative when the U is zero, indicating part of the deposit is dissolved into the solution during T_{off} [20], since zero is above the electrochemical Nernst potential of the redox-reaction [21]

$$Co^{2+} + 2e^{-1} \Leftrightarrow Co$$

which is about -0.5 V as deduced from the Cyclic Voltammetry curve in Fig. 6c. This is beneficial to the recovery of ion concentration near the deposition interface. The delay time further provides additional time for the

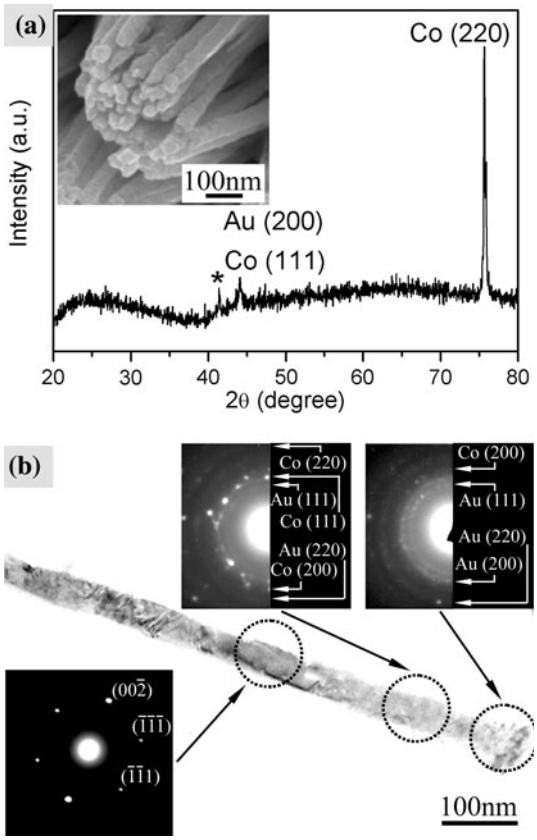

Fig. 5 **a** XRD pattern of the *Co nanowire* array imbedded in AAM, the inset is corresponding FESEM image of the *bottom side* of the nanowires released from the pores of AAM. **b** TEM image of a single *Co nanowire* grown along FCC (220) direction, the insets are the SAED patterns at different positions along the nanowire

concentration of metal ions to recover. This deposition mode favors the growth of existing nuclei instead of formation of new nuclei, thus, perfect crystalline quality and preferentially orientated growth of nanowires can be achieved [11]. However, it is not the case at the initial growth stage of the electrodeposited nanowires. The current at the very beginning of deposition (~5.5 mA) is larger than that in the following process (~3.2 mA), as seen in Fig. 6b. This implies the reduced ions at the initial stage are more than those in the subsequent process, thus the nucleation and growth at the initial stage are less ordered, which is supported by the randomly birthed nuclei in the two systems (rhombohedral Sb nanowire oriented along [110] and FCC Co nanowire oriented along [220]). And this phenomenon seems independent on either the material or the structure.

The active sites for the initial nucleation of metal are randomly distributed due to the polycrystalline feature and roughness surface of the Au substrate, which further facilitates random orientation of the initially formed nanocrystals, as shown schematically in Fig. 7. The nucleation is a progressive process due to slow reduction process in each pulse, and as the deposition proceeds, the

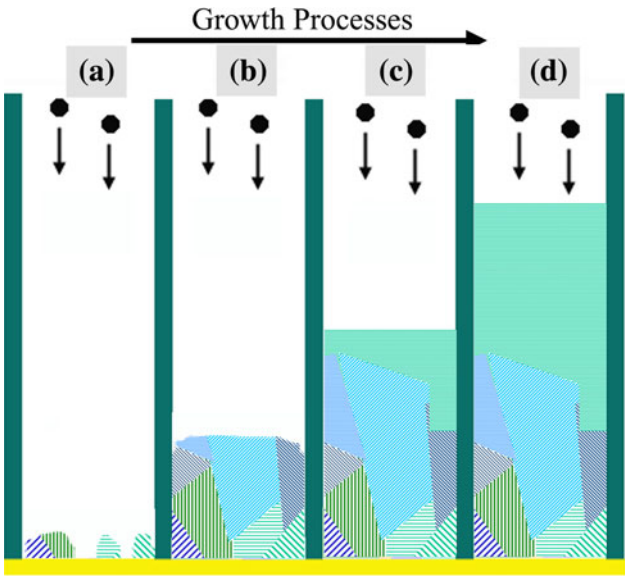

Fig. 7 A sketch of the nucleation and growth processes of metal nanowire grown by pulsed electrodeposition. **a** ions reduction on the *Au electrode* and *random nucleation*, **b** and **c** formation of several *nanocrystals* and *growth in size*, **d** preferred growth of a single crystal along a preferential plane in a *2D growth mode*

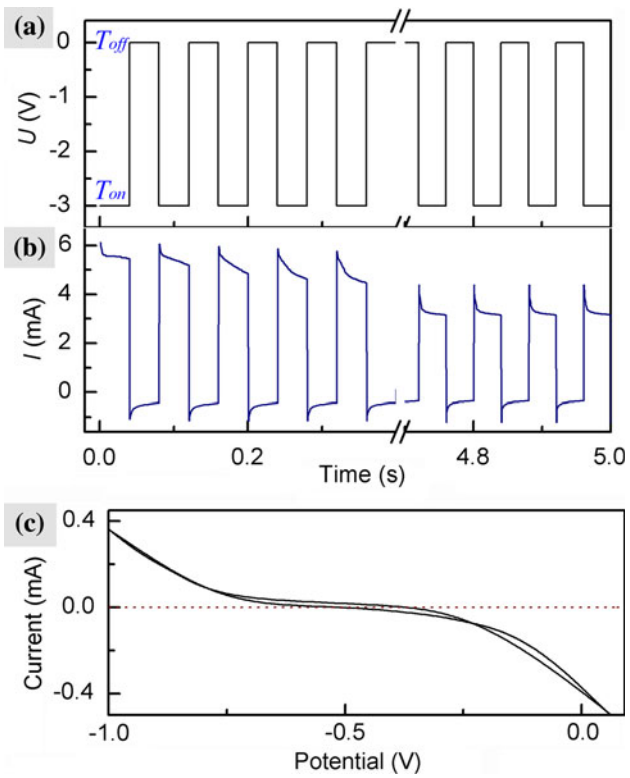

Fig. 6 **a** Real-time deposition potential applied to working electrode (AAM) and **b** the corresponding current–time curve at the initial growth of *Co nanowires*, **c** *Cyclic Voltammetry curve* for *Co nanowires*

nucleus orientated in the direction with low energy surface will grow faster than that with other orientations, resulting its expansion in surface area as more atoms are reduced onto the rough growth front, leading to the transition from heterogeneous nucleation to homogeneous growth process. The growth competition among the adjacent crystal grains and nuclei is inevitable, due to the confined effect of the nanochannels of the AAM [22]. Once the crystal grain with preferential growth direction survives, the subsequent growth will follow its direction according to the two-dimensional (2D) growth mode [23]. This progressive nucleation and 3D-2D growth mechanism is believed to occur through a complex interplay between the lattice strain, surface energy, and surface migration.

It is worth note that the transition length from 3D nucleation to 2D growth is strongly dependent on the local growth environment and growth parameters. It was found that when the pulse deposition time and the delay time were changed to 300 μs and 900 μs, respectively, and keep all the other condition the same as in Fig. 3, the length of the initial 3D growth decreases to about 100 nm, see Fig. 8. The reduced Sb ions at each cycle will decrease with decreasing the pulse deposition time, and thus the Sb atoms have enough time to adjust themselves to a lower energy position due to the increased delay time, leading to the decrease in the length of the initial 3D growth. More detailed study about the orientation dependence of the transition length is needed to further understand the

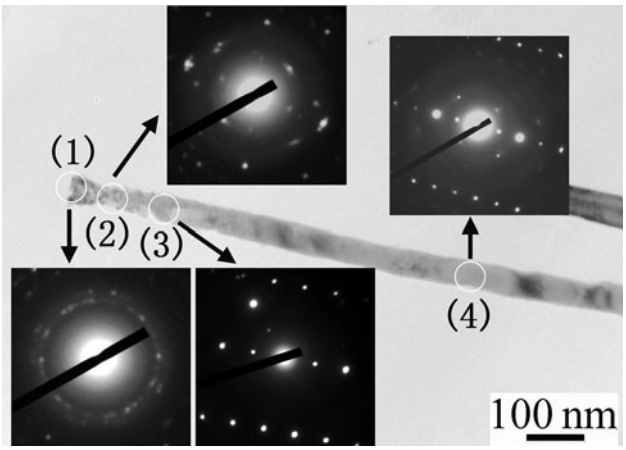

Fig. 8 TEM image of a single Sb nanowire and the corresponding SAED patterns in different areas. The area (1) shows the *Au electrode*, the area (2) shows the *polycrystalline,* and the areas (3) and (4) show *single crystalline*

orientation dependence of the initial growth of the electrodeposited nanowires.

Conclusion

In summary, single-crystalline rhombohedral Sb and FCC Co nanowires with a preferential orientation were synthesized by the pulsed electrodeposition into the pores of AAM, and their initial growth stage were investigated. A transition from 3D nucleation to 2D growth in the initial growth stage was found in the nanoscaled channels, which resulting a structure transition of the nanowires from polycrystalline to single crystalline. We believe this kind of growth behavior is universal in the electrodeposited nanowires.

Acknowledgments This work was supported by the National Natural Science Foundation of China (10704074) and the National Major Project of Fundamental Research for Nanomaterials and Nanostructures (no. 2005CB623603).

References

1. C.M. Lieber, Z.L. Wang, MRS Bull. **32**, 99 (2007)
2. L.E. Greene, M. Law, D.H. Tan, M. Montano, J. Goldberger, G. Somorjai, P.D. Yang, Nano Lett. **5**, 1231 (2005)
3. G.Z. Shen, P.C. Chen, K. Ryu, C.W. Zhou, J. Mater. Chem. **19**, 828 (2009)
4. X.S. Fang, Y. Bando, U.K. Gautam, C.H. Ye, D. Golberg, J. Mater. Chem. **18**, 509 (2008)
5. C.R. Martin, Science **266**, 1961 (1994)
6. K.M. Ryan, D. Erts, H. Olin, M.A. Morris, J.D. Holmes, J. Am. Chem. Soc. **125**, 6284 (2003)
7. Z. Wang, M. Brust, Nanoscale Res. Lett. **2**, 34 (2007)
8. G. Yi, W. Schwarzacher, Appl. Phys. Lett. **74**, 1746 (1999)
9. K.M. Razeeb, F.M.F. Rhen, S. Roy, J. Appl. Phys. **105**, 083922 (2009)
10. X.H. Huang, L. Li, X.C. Dou, G.H. Li, J. Appl. Phys. **105**, 084306 (2009)
11. Y. Zhang, G.H. Li, Y.C. Wu, B. Zhang, W.H. Song, L.D. Zhang, Adv. Mater. **14**, 1227 (2002)
12. F. Qian, Y. Li, S.G. Radečak, H.G. Park, Y. Dong, Y. Ding, Z.L. Wang, C.M. Lieber, Nature Mater. **7**, 701 (2008)
13. H. Yang, W. Luan, S. Tu, Z.M. Wang, Lab Chip **8**, 451 (2008)
14. X.C. Dou, G.H. Li, H.C. Lei, Nano Lett. **8**, 1286 (2008)
15. X.H. Huang, G.H. Li, B.Q. Cao, M. Wang, C.Y. Hao, J. Phys. Chem. C **113**, 4381 (2009)
16. H. Zheng, R.K. Smith, Y. Jun, C. Kisielowski, U. Dahmen, A.P. Alivisatos, Science **324**, 1309 (2009)
17. H. Zheng, S.A. Claridge, A.M. Minor, A.P. Alivisatos, Nano Lett. **9**, 2460 (2009)
18. M. Motoyama, Y. Fukunaka, T. Sakka, Y.H. Ogata, Electrochim. Acta **53**, 205 (2007)
19. E.T.M. Maria, B. Veronique, D. Dobri, N. Reinhard, S. Roland, U.S. Ingrid, V. Johann, Adv. Mater. **13**, 62 (2001)
20. A. Bai, C.C. Hu, Electrochem. Commun. **5**, 78 (2003)
21. W. Schindler, Th Koop, D. Hofmann, J. Kirschner, IEEE Trans. Magn. **34**, 963 (1998)
22. H. Pan, H. Sun, P. Cheekok, Y.P. Feng, J.Y. Lin, Nanotechnology **16**, 1559 (2005)
23. M.L. Tian, J.G. Wang, K. James, E.M. Thomas, M.H.W. Chan, Nano Lett. **3**, 919 (2003)